Biogeosciences Discuss., doi:10.5194/bg-2017-193, 2017
Manuscript under review for journal Biogeosciences
Discussion started: 19 May 2017

Constraints on global oceanic emissions of N_2O from observations and models

Buitenhuis, Erik T.[1, 2], Parvadha Suntharalingam[1], Corinne Le Quéré[1, 2].

[1]School of Environmental Sciences, University of East Anglia, Norwich, United Kingdom

[2]Tyndall Centre for Climate Change Research, University of East Anglia, Norwich, United Kingdom

Correspondence to: Erik T Buitenhuis (E-mail: http://greenocean-data.uea.ac.uk/.feedback.html)

Running head: Ocean N_2O flux

Abstract. We estimate the global ocean N_2O flux to the atmosphere and its confidence interval using a statistical method based on model perturbation simulations and their fit to a database of ΔpN_2O (n=6136). We evaluate two submodels of N_2O production. The first submodel splits N_2O production into oxic and hypoxic pathways following previous publications. The second submodel explicitly represents the redox transformations of N that lead to N_2O production (nitrification and hypoxic denitrification) and N_2O consumption (suboxic denitrification), and is presented here for the first time. We perturb both submodels by modifying the key parameters of the N_2O cycling pathways (nitrification rates, NH_4^+ uptake, N_2O yields under oxic, hypoxic and suboxic conditions), and determine a set of optimal model parameters by minimisation of a cost function against 4 databases of N cycle observations derived from observed and model ΔpN_2O concentrations. Our estimate of the global oceanic N_2O flux resulting from this cost function minimisation is 2.4 ± 0.8 Tg N y^{-1}, and is invariant to the choice of N_2O submodel. These estimates suggest that the currently available observational data of surface ΔpN_2O constrain the global N_2O flux to a narrower range relative to the large range of results presented in the latest IPCC report.

1 Introduction

Nitrous oxide (N_2O) is the third most important contributor to anthropogenic radiative forcing, after carbon dioxide (CO_2) and methane (CH_4) (Myhre et al. 2013). It also currently estimated as the dominant contributor to stratospheric ozone depletion (Portmann et al. 2012). Yet our quantitative understanding of the magnitude and processes controlling natural N_2O emissions from the Earth surface to the atmosphere is very poor. A range of methods have

been used to constrain total oceanic N_2O emissions, including the combination of surface ocean N_2O partial pressure anomalies with gas-exchange parameterizations (Nevison et al. 1995), empirically derived functional relationships applied to global ocean datasets (Nevison et al. 2003, Freing et al. 2012), and ocean biogeochemistry models (Suntharalingam and Sarmiento 2000, Suntharalingam et al. 2000, Jin and Gruber 2003, Martinez-Rey et al. 2015). In spite of the multiple methods used, the reported oceanic emissions of N_2O is still poorly constrained, ranging from 1.9 to 9.4 Tg N y^{-1} according to the latest report of the Intergovernmental Panel on Climate Change (IPCC; Ciais et al. 2013). The uncertainty in the oceanic emissions of N_2O accounts for a large part of the total uncertainty in the natural N_2O emissions, which are approximately 11 Tg N y^{-1} (Ciais et al. 2013).

The large uncertainty in the oceanic emissions of N_2O stems from the complexity of its production pathways. There are two main pathways of N_2O production in the ocean, nitrification and denitrification, which both stem from redox reactions of nitrogen, under oxic and hypoxic conditions, respectively (Fig. 1). N_2O is formed as a byproduct of marine nitrification of ammonium (NH_4^+) to nitrate (NO_3^-); N_2O is also an intermediate product of denitrification, during the reduction of NO_3^- to nitrogen gas (N_2) (Frame and Casciotti 2010, Loescher et al. 2012, Merbt et al. 2012). Denitrification can also consume N_2O, using extracellular N_2O, and reduce it to N_2 (Bange 2008). In the oxic part of the ocean (i.e. most of the ocean, 97% > 34 µmol O_2 L^{-1} (using O_2 data taken from Bianchi et al. 2012)) denitrification is suppressed, and the primary formation pathway is usually ascribed to nitrification (Cohen and Gordon 1978), although there are additional pathways (Klawonn et al. 2015). Oceanic N_2O production in oxic regions is often derived from the linear relationships observed between apparent oxygen utilization (AOU) and apparent N_2O production (ΔN_2O) (e.g. Yoshinari 1976, Cohen and Gordon 1978). However, the ΔN_2O/AOU slope varies in different water masses and oceanic regions (Suntharalingam and Sarmiento 2000). Previous studies have suggested that differences in the ΔN_2O/AOU slope could be driven by changing N_2O yields under varying pressure and temperature (Butler et al. 1989) or varying O_2 concentration (Nevison et al. 2003). Additional mechanisms not yet quantified could include variations in the elemental stoichiometry of the organic matter that is being remineralised, and spatial separation of organic matter remineralisation and nitrification.

Estimates of the contribution from suboxic regions of the ocean (about 3%) to the global N_2O flux vary from net depletion via denitrification (Cohen and Gordon 1978), to 33% for the total N_2O production in the suboxic ocean (Suntharalingam et al. 2012), and to more than 50% from denitrification alone (Yoshida et al. 1989). This ambiguity remains unresolved, and stems from the variation in the ΔN_2O/AOU slope from negative under suboxic conditions,

maximal under hypoxic conditions and lower under oxic conditions (e.g. 0.31 – 0.033 nmol/µmol, Law and Owens 1990).

Here, we estimate the global ocean N_2O flux to the atmosphere and its confidence interval. First, we estimate N_2O flux from observations only (Section 2.1). This estimate has large uncertainty. We subsequently use a statistical approach introduced by Buitenhuis et al. (2013a) to estimate the global oceanic emissions of N_2O and its confidence interval by combining ocean N_2O model simulations with a global database of measurements of surface ΔpN_2O. This approach involves minimisation of a cost function that compares a series of model simulations with a global database of point measurements of surface ΔpN_2O. To achieve this, we use 4 observational databases of the N cycle (Section 2.2). We extend the global ocean biogeochemistry model PlankTOM10 (Le Quéré et al. 2016) with additional N cycle processes, deriving the biogeochemical parameters from the observational databases (Section 2.3-2.4). Then, we describe two separate submodels of different levels of complexity that represent N_2O cycling pathways (Section 2.5-2.7). Finally, estimation of the global oceanic N_2O flux applying the statistical approach to the two submodels is described in Section 3, followed by a discussion of the results (Section 4).

2 Ocean N cycle

2.1 Calculation of global ocean N_2O production from N cycle observations

In this section we provide an initial estimate of global marine N_2O production based on observationally derived quantities characterising marine productivity and the global ocean N cycle. This follows a similar method to Cohen and Gordon (1979), who estimated ocean N_2O production using 'Redfield' type ratios. N_2O is produced either during production of NO_3^- in NH_4^+oxidation or during NO_3^- reduction in denitrification (Fig. 1). We therefore base the N_2O production on total NO_3^- turnover, calculated from primary production times the f-ratio. Primary production (PP) was estimated at 58 ± 7 Pg C y^{-1} (Buitenhuis et al. 2013a). We compiled a database of uptake rates of NO_3^-, NH_4^+ and urea, which gives an average f-ratio of 0.29 ± 0.18 (Fig. 2, large symbols, n=34). The globally averaged ΔN_2O/AOU slope is 81.5 ± 1.4 nmol/mmol (Fig. 3). Finally, since primary production is expressed in carbon terms, and N_2O production was correlated with oxygen (O_2) utilization, we need to include the -O_2:C ratio, which was taken from Anderson & Sarmiento (1994) as 170 ± 10 / 117 ± 14, and the molar weights of C (12) and N in N_2O (28). Thus N_2O production was calculated as PP *f-ratio*-O_2:C *ΔN_2O/AOU. Our best estimate of N_2O production using this method is 58 *1000 * 0.29 * 170/117 * 8.15e-5 *28/12 = 4.6 ± 3.1 Tg N y^{-1}. This estimate lies in the middle of other

reported estimates (see Introduction) but the 68% confidence interval is very large. We therefore investigate the N_2O fluxes using a model optimized with observations in the rest of the paper.

2.2 Observational databases for model development

We used four databases to tune or optimise different aspects of the N cycle in the PlankTOM10 ocean biogeochemistry model. The number of datapoints reported for each database are after gridding to 1º × 1º × 12 months × 33 depths (World Ocean Atlas 2009). The databases used are (1) NH_4^+ specific nitrification rate (n=296) as described in Yool et al. (2007); (2) surface NH_4^+ concentration distribution (n=2713) that combines the dataset used in Paulot et al (2015) with data held by the British Oceanographic Data Centre in January 2014 (Johnson et al. in prep., http://www.bodc.ac.uk); (3) depth-resolved N_2O concentration from the MEMENTO project (n=8047; https://memento.geomar.de/; Bange et al. 2009; downloaded 4 June 2014); and (4) surface partial pressure of N_2O (pN_2O) also from MEMENTO (n=6136; downloaded 16 Sept. 2015). pN_2O was converted to ΔpN_2O using atmospheric pN_2O:

$$pN_2O_{atm} = 0.000009471353376 \times Y^{\wedge 3} - 0.05214713935 \times Y^{\wedge 2} + 95.6806625 \times Y - 58228.4121 \quad (1)$$

(A. Freing, pers. comm., correction to Freing et al. 2009), in which Y is the decimal year.

2.3 Cost Function Formulation

To parameterise the model N cycle, we use a cost function to minimize the difference between model and observations, following the methods of Buitenhuis et al. (2013a):

$$\text{cost function} = 10^{\wedge \text{average}(|10\log(\text{model/observation})|)} \quad (2)$$

This formulation gives equal weight to the relative correspondence between model and observations at small and large observational values. A value of 2 means that, on average, the model deviates from the observations by a factor 2 in either direction. The cost function results for the optimised simulations are summarised in Table 1.

2.4 Nitrification

Our initial biogeochemical model configuration is PlankTOM10 (Le Quéré et al. 2016), which represents growth and loss terms from ten Plankton Functional Types (PFTs), including N_2-fixers, picoheterotrophs (*Bacteria* plus *Archaea*) and denitrification rate, but not denitrifier biomass. A full model description and parameter values were provided in the supplementary material of Le Quéré et al. (2016). Here, we extend the model representation of redox reactions in the N cycle, to create the global biogeochemical model PlankTOM10.2. We describe the new N cycle components below.

In order to represent nitrification rate, the state variable for dissolved inorganic nitrogen was split into NO_3^- and NH_4^+. Respiration by all PFTs produces NH_4^+. The parameterization for nitrification used in our model is based on the analysis of a database of NH_4^+-specific nitrification rates (Yool et al. 2007). Yool et al. (2007) found that observed nitrification rates are highly variable, with no obvious relationship with either latitude or depth. They therefore used a constant rate of 0.2 d^{-1} throughout the ocean in their model. Implementing this rate in our model resulted in a cost function relative to the nitrification rate observations of 4.22 (Table 1). We tested if including temperature, O_2 or light dependence improves the ability of the model to reproduce observed nitrification rates. Regarding the response of ammonia oxidizing *Archaea* (AOA), the main nitrifiers in the ocean (Francis et al. 2005, Wuchter et al. 2006, Loescher et al. 2012), to temperature, we are only aware of the measurements of Qin et al. (2014). These show a ~4-fold variation in maximum growth rate between 3 strains, which poorly constrains the temperature dependence of AOA. We therefore first used a generic Q_{10} of 2 and optimised the rate at 0°C using the nitrification rate observations. This led to a slightly improved representation of the observations (cost function = 4.18). Although the response of AOA and ammonia oxidizing *Bacteria* (AOB) to O_2 has only been measured at 21-25 °C (Frame et al. 2010, Loescher et al. 2012), which limits the range of O_2 concentrations, there was a significant logarithmic relationship between N_2O yield and O_2 (Fig. 4). Implementing this response to O_2 led to a further small improvement of the model nitrification rate relative to the observations (cost=4.16). The response of AOA to light is estimated to be 50% inhibited at 5 µmol photons m^{-2} s^{-1}. However, this estimate is not well constrained (Merbt et al. 2012). Implementing this light response did not improve the model, either in combination with the O_2 and temperature responses or with the temperature response only, and was subsequently omitted. The lack of improvement in nitrification rates by adding light inhibition might reflect the lower sensitivity of AOA to light found by Qin et al. (2014).

2.5 Phytoplankton $K_{½}$ for NH_4^+ uptake

We used the calculation of the preferential uptake of NH_4^+ over NO_3^- by phytoplankton PFTs of Vallina and Le Quéré (2008). The $K_{½}$ of phytoplankton for NH_4^+ has mostly been measured based on uptake rates (syntheses by Goldman and Glibert 1983, and Killberg-Thoreson et al. 2014). Aksnes and Egge (1991) have shown a theoretical expectation of a linear increase of $K_{½}$ with cell radius. The observations are so variable that they neither confirm nor contradict such an increase. Because the model does not include a variable N quota, we need a $K_{½}$ for growth rather than for uptake. The available uptake rate data do not include the supporting data to allow conversion to the $K_{½}$ for

growth. We are only aware of measurements of the $K_{½}$ for growth by Stawiarski (2014). Based on the latter values of 0.09 ± 0.15 µmol/L for picoeukaryotes, the $K_{½}$ of phytoplankton for NH_4^+ was set to 0.1 to 5 µM, increasing linearly with nominal size (Buitenhuis et al. 2013b). The resulting model simulation of surface NH_4^+ concentration increases with latitude, consistent with the observations (Fig. 5). However, due to the highly dynamic nature of NH_4^+ turnover, the ability of the model to reproduce the observed NH_4^+ concentrations at the same times and places was relatively low (cost function=3.3).

2.6 N_2O production

N_2O production is implemented as two distinct submodels that follow a diagnostic and a prognostic approach, respectively. The diagnostic submodel is based on observed ΔN_2O/AOU slopes and has previously been published (Suntharalingam et al. 2000, 2012). In oxic waters it uses one slope to estimate the open ocean source of N_2O production. In hypoxic waters it uses a higher slope to represent the increased yield of N_2O from both nitrification and denitrification in oxygen minimum zones. The hypoxic N_2O yield is maximal at 1 µmol O_2 L^{-1}, and decreases with an e-folding concentration of 10 µmol O_2 L^{-1} (Suntharalingam et al. 2000, 2012).

The prognostic submodel presented here is mechanistic in nature and explicitly represents the primary N_2O formation and consumption pathways associated with the marine nitrogen cycle (Fig. 1). It includes the production of N_2O during oxic nitrification (blue arrows in Fig. 1) and during hypoxic denitrification (red arrow in Fig. 1); and a consumption term during denitrification at even lower (suboxic) O_2 concentrations (yellow arrow in Fig. 1). The slopes of the three processes are globally invariant. The slopes of both submodels were optimized using the databases of observed N_2O concentration and ΔpN_2O (see Sections 3.1 and 3.2).

2.7 N_2O flux and simulation setup

N_2O is transported like other tracers. The solubility of N_2O is calculated using the formulation from Weiss and Price (1980). N_2O flux (=air-sea gas exchange) is calculated with the piston velocity from Sweeney et al. (2007), which is optimised for use with the NCEP reanalysis data used here. The Schmidt number for N_2O was taken from Wanninkhof et al. (1992).

The PlankTOM10.2 biogeochemical model coupled with the two N_2O submodels is incorporated into the ocean general circulation model NEMO v3.1 (Madec 2008). The model resolution is 2° in longitude, on average 1.1° in latitude and has 30 vertical layers, from 10 m in the top 100 m to 500 m at 5000 m. The model simulations were initialised in 1965 from observations (Le Quéré et al. 2016), with NH_4^+ initialised as 0, and N_2O initialised from a

Biogeosciences Discuss., doi:10.5194/bg-2017-193, 2017
Manuscript under review for journal Biogeosciences
Discussion started: 19 May 2017

horizontal interpolation of the MEMENTO observations (see Section 2.2). Simulations were run to 2014, forced with daily atmospheric conditions from the NCEP reanalysis (Kalnay et al. 1996), (for details see Buitenhuis et al. 2013a). Results are reported averaged over the last 5 years.

2.8 Estimation of global N_2O flux from point measurements of ΔpN_2O

To estimate the global air-sea flux of N_2O that best fits the ΔpN_2O data, and its ±1-sigma (68%) confidence interval, we use the formula described in Buitenhuis et al. (2013a):

$$RSS/RSS_{min} = 0.468 \times n/(n-2) \times \sqrt{(2(2n-2)/(n(n-4)))} + n/(n-2) \quad (3)$$

in which RSS is the residual sum of squares between each model simulation and the observations, RSS_{min} is the RSS of the model simulation that is closest to the observations, and n is the number of observations.

To estimate the influence that inequality of model means and the observational mean have on the validity of using equation 3, we use equation 2.1 from Donaldson (1968), with the observational database taken as the "parent" or "true" distribution:

$$\varphi = \sqrt{(n^2 \times (\overline{observations} - \overline{model})^2/RSS)} \quad (4)$$

3 Results

3.1 N_2O production at low O_2

The global N_2O production rate in oxygen minimum zones (OMZs) was optimized using the depth-resolved N_2O data of the MEMENTO database. As noted in previous model studies of ocean O_2, global models do not well represent the extent and intensity of OMZ regions (Bopp et al. 2013, Cocco et al. 2013, Andrews et al. 2016). The modeled OMZs in PlankTOM10 occur at greater depths than observed, resulting in unrealistic vertical distributions of N_2O (results not shown). Therefore, following Suntharalingam et al. (2012), the model was run using fixed observed O_2 concentrations (Bianchi et al. 2012), which corrected, in part, the vertical distribution of N_2O production from the two submodels, though it still occurred at too great depths (Fig. 6). In the equatorial regions and in the Pacific ocean the N_2O concentrations are underestimated between ~200 and ~1500 m. depth, and overestimated below that. This shortcoming is not significantly improved in the prognostic model (Fig. 6), even though the prognostic model represents the process of N_2O consumption at low O_2 concentrations. The depth of maximum N_2O in the model is generally deeper than observed, suggesting that organic matter remineralisation may be too low at shallow depths. This is confirmed by the depth profile of NO_3^-, which is underestimated relative to the WOA2009

observations between 100 and 1500 m., and overestimated at greater depths (Fig. 7). In both submodels, the N_2O concentrations in the deep sea are also too high, but since only 5% of N_2O production occurs below 1600 m this does not have a big impact on the global N_2O fluxes. The addition of N_2O consumption in the prognostic N_2O model does result in improvement of the N_2O depth profiles in the Indian Ocean.

In order to find the optimal N_2O production that minimizes the RSS (Eq. 3), we ran a range of simulations in which the low O_2 N_2O production was varied in the diagnostic model (Fig. 8A), and a range of simulations in which both the hypoxic N_2O production and the suboxic N_2O consumption were varied in the prognostic model (Fig. 8B). The optimum solution for the prognostic model was found at a gross production of 0.33 Tg N y^{-1}. The optimised N_2O production in low O_2 regions and its confidence interval were 0.16 ± 0.13 Tg N y^{-1} for the diagnostic model, and 0.12 ± 0.07 Tg N y^{-1} for the prognostic model. In the optimized diagnostic model the hypoxic N_2O slope is 0.0017 mol N_2O/mol O_2. In the optimized prognostic model the maximum N_2O consumption slope is 0.015 mol N_2O (mol $NO_3^-)^{-1}$, decreasing to 0 above 28 µmol O_2 L^{-1}. The maximum N_2O production slope is 0.0154 mol N_2O (mol $NO_3^-)^{-1}$ decreasing to 0 above 34 µmol O_2 L^{-1}. This leads to net production that is always positive and has a maximal slope of 183 µmol N_2O (mol $NO_3)^{-1}$ at 10 µmol O_2 L^{-1}.

3.2 N_2O flux

We used the surface ΔpN_2O distribution to constrain the total global N_2O flux. ΔpN_2O provided a better constraint than the N_2O concentration distribution, since more N_2O production mostly leads to more N_2O outgassing to the atmosphere rather than a significant increase in shallow N_2O concentrations (data not shown). The zonal average surface ΔpN_2O distribution was well simulated by both submodels (Fig. 9D), and the model ensemble covered a wide range of global N_2O fluxes (Fig. 10). The total N_2O flux that best reproduced the ΔpN_2O distribution was 2.40 ± 0.29 Tg N y^{-1} for the diagnostic sub-model and 2.44 ± 0.29 Tg N y^{-1} for the prognostic sub-model (Fig. 10). In the diagnostic model, the optimized oxic ΔN_2O/AOU slope was 12.7 µmol N_2O (mol $O_2)^{-1}$. In the prognostic model, the optimized nitrification slope was 145 µmol N_2O (mol $NH_4^+)^{-1}$.

In addition to the uncertainty that arises from the model-observations mismatch, uncertainty is contributed by the uncertainties in the N_2O solubility and the piston velocity, the two quantities that connect the measured ΔpN_2O to the estimated air-sea flux. The uncertainty in the solubility has been estimated as 3% (Cohen and Gordon 1978). The uncertainty in the piston velocity has been estimated at 32% (Sweeney et al. 2007). Uncertainties in the solubility and piston velocity are proportional to uncertainty in the optimized N_2O air-sea exchange because the

optimized N_2O production needs to change proportionally with solubility and piston velocity to achieve the same ΔpN_2O. Through error propagation, this gives a total uncertainty of 2.4 ± 0.8 Tg N y^{-1} for both sub-models.

4 Discussion

Cohen and Gordon (1979) estimated global N_2O production directly from N-cycle observations. However, they did not have information on the f-ratio, so their estimate was based on total N assimilation in primary production. Suntharalingam et al. (2012) note that N_2O production is proportional to export production. However, this is dependent on the model formulation, which was based on earlier studies that suggested nitrification in the ocean surface layer was light-inhibited (e.g., Horrigan, 1981). More recent analyses of nitrification, e.g., the database of Yool et al. (2007) find widespread nitrification in the upper mixed layer. In light of this, we decided to recalculate the N cycle based N_2O production based on currently available data. We find that we can estimate all the relevant steps in the N cycle with observational data, including their uncertainty (Section 2.1). At present this uncertainty is still fairly large, at 4.6 ± 3.1 Tg N yr^{-1}. The biggest contributor to this uncertainty is the f-ratio, especially in the tropics, which constitute 44% of the ocean surface area. The f-ratio data is only based on uptake of NO_3^-, NH_4^+ and urea, whereas phytoplankton can also take up NO_2^- and organic N (other than urea). One of the major sources of uncertainty in using the ΔN_2O/AOU ratio is that it is conceptually based on the N_2O production during nitrification, which uses O_2. N_2O production during denitrification is spatially separated from the associated O_2 use that is needed to nitrify the NO_3^-, the electron donor in denitrification. This NO_3^- is produced by nitrification, so in terms of mass balance our calculation is still valid, but this N_2O production would show up as a vertical increase in N_2O without associated increase in AOU at low O_2 concentrations (high AOU) in Figure 3. This estimate of global marine N_2O production derived from analyzing the N cycle currently has a much larger error than the N_2O flux derived from ΔpN_2O observations, but further observational constraints could further our understanding of the whole N cycle, including the option of evaluating their model representation against observations, and not just the part that N_2O plays in them. Such further constraints are also likely to provide the most productive way to reduce unexplained variability that is found in the observations but not in the present models.

Models of the global marine C cycle have been in use for decades, and a lot of the available information has been synthesized, cross-correlated and interpreted in detail. While actual measurements of N utilisation and transformation have also been made in abundance, the synthesis and global modelling of these data is less advanced.

In addition, N occurs in many different oxidation states in the marine environment (e.g. organic matter and NH_4^+ as -3, N_2 as 0, N_2O as 0 and +2, NO_2^- as +3, and NO_3^- as +5). Therefore, redox reactions complicate the representation of the N cycle a good deal. This lack of data synthesis and of identification of the most important controls in a complex system is reflected in a relatively low ability of the model to model observed nitrification rates and NH_4^+ concentrations (Table 1).

This lack of knowledge also means that partitioning the global marine N_2O production over the nitrification and denitrification pathways is poorly constrained. Both the diagnostic and the prognostic models assign a small percentage of the total N_2O production to the denitrification pathway, 6 and 4% respectively. However, because of the large bias between the observed and modeled N_2O concentration depth profiles (Fig. 6) these may be underestimates. Possibly because of the model bias (Fig. 6, 7), the addition of N_2O consumption in the prognostic submodel does not lead to a significantly better distribution of N_2O across depth or between different basins (Fig. 7). As a result, the ΔpN_2O distributions are also quite similar (Fig. 9, 12) and the optimized N_2O flux and confidence intervals of the two submodels are also quite similar (Fig. 10). It should also be noted, however, that the optimization using surface ΔpN_2O agrees with the optimization using N_2O concentration that the contribution of the low O_2 N_2O production needs to be low (Fig. 10), and the error contribution from the model vs. observed ΔpN_2O comparison is also low with confidence intervals of 0.29 Tg N y^{-1} for both submodels, confirming the visual impression that ΔpN_2O is equally well modelled above the low O_2 regions as in the rest of the ocean (Fig. 9, 12). Two complementary approaches could provide better constraints: a better representation of the vertical distribution of export and remineralisation would allow the optimization against N_2O concentration observations to achieve better results. But conversely, with better constraints on the physiology of nitrifiers and denitrifiers the N_2O concentration database could provide constraints on the representation of remineralisation.

Despite these shortcomings, the global marine N_2O flux is well constrained to 2.4 ± 0.8 Tg N y^{-1} by both submodels (Fig. 10). This reflects the fact that the integrated effect of the different physical and biogeochemical processes determines the surface ΔpN_2O distribution (Fig. 9). The N_2O flux is at the lower end of previous estimates, and with a similar confidence interval to other recent estimates (Fig. 11). The confidence interval is dominated by uncertainty in the piston velocity (32%) rather than model-observation mismatches (12%).

Modeled ΔpN_2O values from the optimized simulations of the diagnostic and prognostic submodels have a small negative bias relative to the observations of -2.4 ppb for the diagnostic submodel and -2.7 ppb for the

prognostic submodel (Fig. 12). This gives a degree of inequality (φ, Eq. 4) between the means of the observations and the diagnostic submodel of 0.41 and the prognostic submodel of 0.46. This is well within the range where even much smaller sample sizes lead to negligible Type I errors and conservative Type II errors (Donaldson 1968).

We also tested how much influence sampling biases of very high supersaturation values might have on the estimated air-sea exchange. If the 40 ΔpN_2O measurements in the gridded database that are higher than 100 ppb (Fig. 12) are doubled, the optimized N_2O air-sea exchange becomes 2.9 ± 1.0 Tg N y^{-1} for the diagnostic model and 3.0 ± 1.1 Tg N y^{-1} for the prognostic model. If the 27 ΔpN_2O measurements in the gridded database that are higher than 140 pm are excluded, to decrease the frequency of the highly oversaturated observations down to what the diagnostic model simulates (Fig. 12), the optimized N_2O flux becomes 2.2 ± 0.7 Tg N y^{-1} for both submodels. These results still fall within the confidence intervals of the results using the complete database.

Possible biases in ocean physical transport could in theory affect N_2O production in low O_2 regions. However the model results do not suggest strong biases in N_2O production as a result. On the one hand, if the model had too much ventilation in the OMZs, shallow N_2O concentrations would be underestimated, as they are in the model (Fig. 6), but this would also lead to ΔpN_2O overestimation in the surface areas above the OMZs, which is not the case; the high ΔpN_2O are generally lower but spread over a larger area than in the observations (Fig. 9), with a good frequency distribution of high ΔpN_2O (Fig. 12). On the other hand, if the model had too little ventilation in the OMZs, the optimization would reduce N_2O production in the OMZs in compensation, but the optimization to ΔpN_2O would then estimate a higher OMZ N_2O production than the optimization to the N_2O depth profiles to compensate for the low transport, and this is also not the case. Therefore we conclude that potential biases in ocean physical transport do not appear to have large direct impact on low N_2O production. The indirect impact of ocean physics on low N_2O production through its impact on the distribution of O_2, which Zamora and Oschlies (2014) have shown to be substantial, is not quantified here because we used observed O_2 (Bianchi et al. 2012) instead of modeled O_2.

Global oceanic N_2O emissions estimated using atmospheric inversion methods based on atmospheric N_2O concentrations tend to be higher than our results (Fig. 11). However, N_2O emissions from inversions are low in the Southern Ocean (Hirsch et al. 2006, Huang et al. 2008, Thompson et al. 2014, Saikawa et al. 2014), consistent with our results. South of 30°S, 88% of the Earth surface is ocean, resulting in a clear attribution of the atmospheric N_2O anomalies to ocean fluxes. We suggest that the higher emissions estimates from inversions could be due to a combination of overestimated priors of ocean fluxes in combination with insufficient observational constraints at

latitudes North of 30°S to allow correct partitioning between land and ocean fluxes. Results presented here are for the open and coastal ocean and do not include estuaries; fluxes from these could be as large as 2.3 – 3.6 Tg N y^{-1} according to one estimate (Bange et al. 1996), and could be another contributing factor to the difference between our results and those of atmospheric inversions.

Acknowledgements

This research was supported by the European Commission's Horizon 2020 programme through the CRESCENDO and EMBRACE projects (projects 641816 and 282672). We thank Martin Johnson for the database of NH_4^+, and Andrew Yool for the database of nitrification rates. The MEMENTO database is administered by the Kiel Data Management Team at GEOMAR Helmholtz Centre for Ocean Research and supported by the German BMBF project SOPRAN (Surface Ocean Processes in the Anthropocene, http://sopran.pangaea.de). The four databases presented in this manuscript are available as NetCDF files from https://www.uea.ac.uk/green-ocean/data.

References

Aksnes, D. L., J. K. Egge (1991) A theoretical model for nutrient uptake in phytoplankton. Marine Ecol. Progr. Ser. **70**:65-72

Anderson, L. A., J. L. Sarmiento (1994) Redfield ratios of remineralization determined by nutrient data analysis. Global Biogeochemical Cycles 8: 65-80

Bange, H. W., S. Rapsomanikis, and M. O. Andreae (1996) Nitrous oxide in coastal waters, Global Biogeochem. Cycles 10: 197– 207, doi:10.1029/95GB03834.

Bange, H. (2008) Gaseous nitrogen compounds (NO, N_2O, N_2, NH_3) in the ocean. *In*: Nitrogen in the marine environment (eds D. G. Capone, D. A. Bronk, M. R. Mulholland, E. J. Carpenter), p. 51–94, New York, NY: Elsevier.

Bange, H. W., Bell, T. G., Cornejo, M., Freing, A., Uher, G., Upstill-Goddard, R. C., and Zhang, G. L. (2009) MEMENTO: a proposal to develop a database of marine nitrous oxide and methane measurements, Environmental Chemistry 6: 195-197, doi:10.1071/en09033.

Bianchi, D., J. P. Dunne, J. L. Sarmiento, E. D. Galbraith (2012) Data-based estimates of suboxia, denitrification, and N2O production in the ocean and their sensitivity to dissolved O2, Glob. Biogeochem. Cycles 26, GB2009, doi:10.1029/2011GB004209.

Buitenhuis, E. T., Hashioka, T., Le Quéré, C. (2013a) Combined constraints on global ocean primary production using observations and models. Global Biogeochemical Cycles 27: 847-858

Buitenhuis, E. T., M. Vogt, R. Moriarty, N. Bednaršek, S. Doney, K. Leblanc, C. Le Quéré, Y.-W. Luo, C. O'Brien, T. O'Brien, J. Peloquin, R. Scheibel (2013b) MAREDAT : towards a World Ocean Atlas of marine ecosystem data. Earth System Science Data 5: 227-239, doi:10.5194/essd-5-227-2013.

Butler, J. H., J. W. Elkins, T. M. Thompson, K. B. Egan (1989) Tropospheric and dissolved N2O of the West Pacific and East Indian Oceans during the El Niño Southern Oscillation event of 1987, J. Geophys. Res. 94: 14865-14877.

Ciais, P., C. Sabine, G. Bala, L. Bopp, V. Brovkin, J. Canadell, A. Chhabra, R. DeFries, J. Galloway, M. Heimann, C. Jones, C. Le Quéré, R. B. Myneni, S. Piao and P. Thornton (2013) Carbon and Other Biogeochemical Cycles. In: Climate Change 2013: The Physical Science Basis. Contribution of Working Group I to the Fifth Assessment Report of the Intergovernmental Panel on Climate Change [Stocker, T.F., D. Qin, G.-K. Plattner, M. Tignor, S.K.

Allen, J. Boschung, A. Nauels, Y. Xia, V. Bex and P.M. Midgley (eds.)]. Cambridge University Press, Cambridge, United Kingdom and New York, NY, USA, pp. 465-570, doi:10.1017/CBO9781107415324.015.

Cohen, Y., L. I. Gordon (1978) Nitrous oxide in the oxygen minimum of the eastern tropical North Pacific: evidence for its consumption during denitrification and possible mechanisms for its production. Deep-Sea Res. 25: 509-524.

Cohen, Y., and L. I. Gordon (1979) Nitrous oxide production in the ocean. J. Geophys. Res. 84: 347-353

Donaldson, T. S. (1968) Robustness of the F-test to errors of both kinds and the correlation between the numerator and the denominator of the F-ratio. J. Amer. Statist. Assoc. 63: 660-676.

Frame, C. H., K. L. Casciotti (2010) Biogeochemical controls and isotopic signatures of nitrous oxide production by a marine ammonia-oxidizing bacterium. Biogeosciences 7: 2695-2709, .

Francis, C. A., K. J. Roberts, J. M. Beman, A. E. Santoro, and B. B. Oakley (2005) Ubiquity and diversity of ammonia-oxidizing archaea in water columns and sediments of the ocean. PNAS 102: 14683-14688, doi: 10.1073/pnas.0506625102,

Freing , A. D. W. R. Wallace, T. Tanhua, S. Walter, H. W. Bange (2009) North Atlantic production of nitrous oxide in the context of changing atmospheric levels. Global Biogeochemical Cycles 23, GB4015, doi:10.1029/2009GB003472,

Freing , A. D. W. R. Wallace, H. W. Bange (2012) Global oceanic production of nitrous oxide. Phil. Trans. R. Soc. 367: 1245-1255, doi: 10.1098/rstb.2011.0360,

Gandhi, N., R. Nameesh, R. Srivastava, M. S. Sheshshayee, R. M. Dwivedi, M. Raman (2010) Nitrogen uptake rates during spring in the NE Arabian Sea. International Journal of Oceanography 2010: 127493, doi: 10.1155/2010/127493,

Gandhi, N., R. Nameesh, A. H. Laskar, M. S. Sheshshayee, S. Shetye, N. Anilkumar, S. M. Patil, R. Mohan (2012) Zoanal variability in primary production and nitrogen uptake rates in the southwestern Indian Ocean and the Southern Ocean. Deep Sea Res I 67: 32-43, doi:10.1016/j.dsr.2012.05.003,

Goldman, J. C., P. M. Glibert (1983) Kinetics of inorganic nitrogen uptake by phytoplankton. *In*: Nitrogen in the marine environment, Carpenter, E. J. and D. G. Capone (eds.) Elsevier,

Goreau, T. J., W. A. Kaplan, S. C. Wofsy, M. B. McElroy, F. W. Valois, S. W. Watson (1980) Production of NO2- and N2O by nitrifying bacteria at reduced concentrations of oxygen. Appl. Env. Microbiol. 40: 526-532,

Hirsch, A. I., A. M. Michalak, L. M. Bruhwiler, W. Peters, E. J. Dlugokencky, and P. P. Tans (2006) Inverse modeling estimates of the global nitrous oxide surface flux from 1998–2001, Global Biogeochem. Cycles 20, GB1008, doi:10.1029/2004GB002443,

Horrigan, S. G., A. F. Carlucci, P. M. Williams (1981) Light inhibition of nitrification in sea-surface films. J. Mar. Res. 39: 557-565,

Huang, J., A. Golombek, R. Prinn, R. Weiss, P. Fraser, P. Simmonds, E. J. Dlugokencky, B. Hall, J. Elkins,P. Steele, R. Langenfelds, P. Krummel, G. Dutton, and L. Porter (2008) Estimation of regional emissions of nitrous oxide from 1997 to 2005 using multinetwork measurements, a chemical transport model, and an inverse method, J. Geophys. Res. 113, D17313, doi:10.1029/2007JD009381,

Jin, X., N. Gruber (2003) Offsetting the radiative benefit of ocean iron fertilization by enhancing N2O emissions. Geophysical Research Letters 30, 2249, doi:10.1029/2003GL018458,

Joubert, W. R., S. J. Thomalla, H. N. Waldron, M. I Lucas, M. Boye, F. A. C. Le Moigne, F. Planchon, S. Speich (2011) Nitrogen uptake by phytoplankton in the Atlantic sector of the Southern Ocean during late austral summer. Biogeosciences 8:2947-2959, doi:10.5194/bg-8-2947-2011,

Kalnay, E., M. Kanamitsu, R. Kistler, W. Collins, D. Deaven, L. Gandin, M. Iredell, S. Saha, G. White, J. Woollen, Y. Zhu, M. Chelliah, W. Ebisuzaki, W. Higgins, J. Janowiak, K. C. Mo, C. Ropelewski, J. Wang, A. Leetmaa, R. Reynolds, R. Jenne, and D. Joseph (1996) The NCEP/NCAR 40-year reanalysis project. *Bull. Am. Meteorol. Soc.* 77(3), 437-471,

Killberg-Thoreson, L., M. R. Mulholland, C. A. Heil, M. P. Sanserson, J. M. O'Neil, D. A. Bronk (2014) Nitrogen uptake kinetics in field populations and cultured strains of *Karenia brevis*. Harmful Algae 38: 73-85, doi:10.1016/j.hal.2014.04.008,

Law, C.S., and N. J. P. Owens (1990) Significant flux of atmospheric nitrous-oxide from the Northwest Indian Ocean. Nature, 346: 826-828, doi:10.1038/346826a0,

Le Quéré, C., E. T. Buitenhuis, R. Moriarty, S. Alvain, O. Aumont, L. Bopp, S. Chollet, C. Enright, D. J. Franklin, R. J. Geider, S. P. Harrison, A. Hirst, S. Larsen, L. Legendre, T. Platt, I. C. Prentice, R. B. Rivkin, S. Sailley, S. Sathyendranath, N. Stephens, M. Vogt, and S. M. Vallina (2016) Role of zooplankton dynamics for Southern Ocean phytoplankton biomass and global biogeochemical cycles. Biogeosciences 13: 4111-4133, doi:10.5194/bg-13-4111-2016, .

Lipschultz, F. O. C. Zafiriou, S. C. Wofsy, et al. (1981) Production of NO and N_2O by soil nitrifying bacteria. Nature 294: 641-643, .

Loescher, C. R., A. Kock, M. Koenneke, J. LaRoche, H. W. Bange, R. A. Schmitz (2012) Production of oceanic nitrous oxide by ammonia-oxidizing archaea. Biogeosciences 9: 2419-2429, .

Madec, G. (2008) NEMO ocean engine. Note du Pole de modélisation, Institut Pierre-Simon Laplace (IPSL), France, No 27 ISSN No 1288-1619. http://www.nemo-ocean.eu/content/download/21612/97924/file/NEMO_book_3_4.pdf,

Merbt, S. N., D. A. Stahl, E. O. Casamayor, et al. (2012) Differential photoinhibition of bacterial and archaeal ammonia oxidation. FEMS microbiology letters 327: 41-46, .

Myhre, G., D. Shindell, F.-M. Bréon, W. Collins, J. Fuglestvedt, J. Huang, D. Koch, J.-F. Lamarque, D. Lee, B. Mendoza, T. Nakajima, A. Robock, G. Stephens, T. Takemura and H. Zhang (2013) Anthropogenic and Natural Radiative Forcing. *In*: Climate Change 2013: The Physical Science Basis. Contribution of Working Group I to the Fifth Assessment Report of the Intergovernmental Panel on Climate Change [Stocker, T.F., D. Qin, G.-K. Plattner, M. Tignor, S.K. Allen, J. Boschung, A. Nauels, Y. Xia, V. Bex and P.M. Midgley (eds.)]. Cambridge University Press, Cambridge, United Kingdom and New York, NY, USA, pp. 659-740, doi:10.1017/CBO9781107415324.018, .

Nevison, C. D., R. F. Weiss, D. J Erickson III (1995) Global oceanic emissions of nitrous oxide. J. Geophys. Res. 100: 15809-15820, .

Nevison, C., J. H. Butler, J. W. Elkins (2003) Global distribution of N2O and the ΔN2O-AOU yield in the subsurface ocean. Glob. Biogeochem. Cycles 17: 1119, doi:10.1029/2003GB002068,

Paulot, F., D.J. Jacob, M. T. Johnson,T.G. Bell, A. R. Baker, W. C. Keene, I. D. Lima, S. C. Doney, and C. A. Stock (2015) Global oceanic emission of ammonia: Constraints from seawater and atmospheric observations. Glob. Biogeochem. Cycles, 29: 1165–1178, doi:10.1002/2015GB005106,

Portmann, R. W., J. S. Daniel, and A. R. Ravishankara (2012) Stratospheric ozone depletion due to nitrous oxide: influences of other gases. Phil. Trans. R. Soc. B, 367: 1256–1264, doi:10.1098/rstb.2011.0377,

Prakash, S., R. Ramesh, M. S. Sheshshayee, R. M. Dwivedi, M. Raman (2008) Quantification of new production during a winter *Noctiluca scintillans* bloom in the Arabian Sea. Geophys. Res. Letters 35, L08604, doi:10.1029/2008GL033819,

Prakash, S., R. Ramesh, M. S. Sheshshayee, R. Mohan, M. Sudhakar (2015) Nitrogen uptake rates and f-ratios in the Equatorial and Southern Indian Ocean. Current Science 108: 239-245,

Saikawa, E., R. G. Prinn, E. Dlugokencky, K. Ishijima, G. S. Dutton, B. D. Hall, R.Langenfelds, Y. Tohjima, T. Machida, M. Manizza, M. Rigby, S. O'Doherty, P. K. Patra, C. M. Harth, R. F. Weiss, P. B. Krummel, M. van der Schoot, P. J. Fraser, L. P. Steele, S. Aoki, T. Nakazawa, and J. W. Elkins (2014) Global and regional emissions estimates for N2O, Atmos. Chem. Phys. 14: 4617-4641, doi:10.5194/acp-14-4617-2014,

Simpson, K. G., J.-E. Tremblay, S. Brugel, N. M. Price (2013) Nutrient dynamics in the western Canadian Arctic. Mar. Ecol. Progr. Ser. 484:47-62, doi:10.3354/meps10298,

Stawiarski, B. (2014) The physiological response of picophytoplankton to light, temperature and nutrients, including climate change model simulations. PhD thesis, University of East Anglia, https://ueaeprints.uea.ac.uk/53423/1/2014StawiarskiBPhD.pdf,

Suntharalingam, P., J. L. Sarmiento (2000) Factors governing the oceanic nitrous oxide distribution: Simulations with an ocean general circulation model. Global Biogeochemical Cycles 14: 429-454,

Suntharalingam, P., J. L. Sarmiento, and J. R. Toggweiler (2000) Global significance of nitrous-oxide production and transport from oceanic low-oxygen zones: A modeling study, Global Biogeochem. Cycles, 14: 1353–1370, doi:10.1029/1999GB900100,

Suntharalingam, P., Buitenhuis, E., Le Quere, C., Dentener, F., Nevison, C., Butler, J., Bange, H., Forster, G. (2012) Quantifying the Impact of Anthropogenic Nitrogen Deposition on Oceanic Nitrous Oxide in Geophysical Research Letters 39, L07605, doi:10.1029/2011GL050778,

Thomalla, S. J., H. N. Waldron, M. I. Lucas, J. F. Read, I. J. Ansorge, E. Pakhomov (2011) Phytoplankton distribution and nitrogen dynamics in the southwest Indian subtropical gyre and Southern Ocean waters. Ocean Sci. 7: 113-127, doi:10.5194/os-7-113-2011,

Thompson, R. L., F. Chevallier, A. M. Crotwell, G. Dutton, R. L. Langenfelds, R. G. Prinn, R. F. Weiss, Y. Tohjima, T. Nakazawa, P. B. Krummel, L. P. Steele, P. Fraser, S. O'Doherty, K. Ishijima, and S. Aoki (2014) Nitrous oxide emissions 1999 to 2009 from a global atmospheric inversion, Atmos. Chem. Phys. 14: 1801-1817, doi:10.5194/acp-14-1801-2014,

Vallina, S. M., C. Le Quere (2008) Preferential uptake of NH_4^+ over NO_3^- in marine ecosystem models: A simple and more consistent parameterization. Ecol. Model. 218: 393-397,

Varela, M. M., A. Bode, E. Fernandez, N. Gonzalez, V. Kitidis, M. Varela, E. M. S. Woodward (2005) Nitrogen uptake and dissolved organic nitrogen release in planktonic communities characterised by phytoplankton size-structure in the Central Atlantic Ocean. Deep Sea Res. I 52: 1637-1661 doi:10.1016/j.dsr.2005.03.005,

Varela, D. E., D. W. Crawford, I. A. Wrohan, S. N. Wyatt, E. C. Carmack (2013) Pelagic primary productivity and upper ocean nutrient dynamics across Subarctic and Arctic Seas. J. Geophys. Res. 118: 7132-7152, doi:10.1002/2013JC009211,

Wafar, M., S. L'Helguen, V. Raikar, J-F. Maguer, P. Le Corre (2004) Nitrogen uptake by size-fractionated plankton in permanently well-mixed temperate coastal waters. J. Plankton Res. 26:1207-1218, doi:10.1093/plankt/fbh110,

Wanninkhof, R. (1992) Relationship between wind speed and gas exchange over the ocean. J. Geophys. Res. 97:7373-7382, .

Weiss, R. F., B. A. Price (1980) Nitrous oxide solubility in water and seawater. Mar. Chem. 8: 347-359, .

Wuchter, C., B. Abbas, M. J. L. Coolen, L. Herfort, J. van Bleijswijk, P. Timmers, M. Strous, E. Teira, G. J. Herndl, J. J. Middelburg, S. Schouten, and J. S. Sinninghe Damsté (2006) Archaeal nitrification in the ocean. PNAS 103: 12317-12322, doi: 10.1073/pnas.0600756103,

Yool, A., A. P. Martin, C. Fernandez, et al. () The significance of nitrification for oceanic new production. Nature 447: 999-1002, 2007.

Yoshinari, T. () Nitrous oxide in the sea. Marine Chemistry 4: 189-202, 1976.

Biogeosciences Discuss., doi:10.5194/bg-2017-193, 2017
Manuscript under review for journal Biogeosciences
Discussion started: 19 May 2017

Table, Figures and captions

Table 1: Cost function (Equation 2) for the optimisation simulations of sections 2.2-2.4, relative to the respective observational databases. The nitrification rate in bold was used in this study.

Database	Model change	Cost function
Nitrification rate	0.2 d^{-1}	4.22
	0.1 $d^{-1} * 2^{\wedge(T/10)}$	4.18
	0.79 $d^{-1} * 2^{\wedge(T/10)}*(1-0.159*\ln(O_2))$	**4.16**
	0.58 $d^{-1} * 2^{\wedge(T/10)}*e^{\wedge(-0.14*I)}$	7.15
	4.7 $d^{-1} * 2^{\wedge(T/10)}*(1-0.159*\ln(O_2)) *e^{\wedge(-0.14*I)}$	6.87
Surface NH_4^+ concentration	$K_{½}$ estimated from observations	3.3

Biogeosciences Discuss., doi:10.5194/bg-2017-193, 2017
Manuscript under review for journal Biogeosciences
Discussion started: 19 May 2017

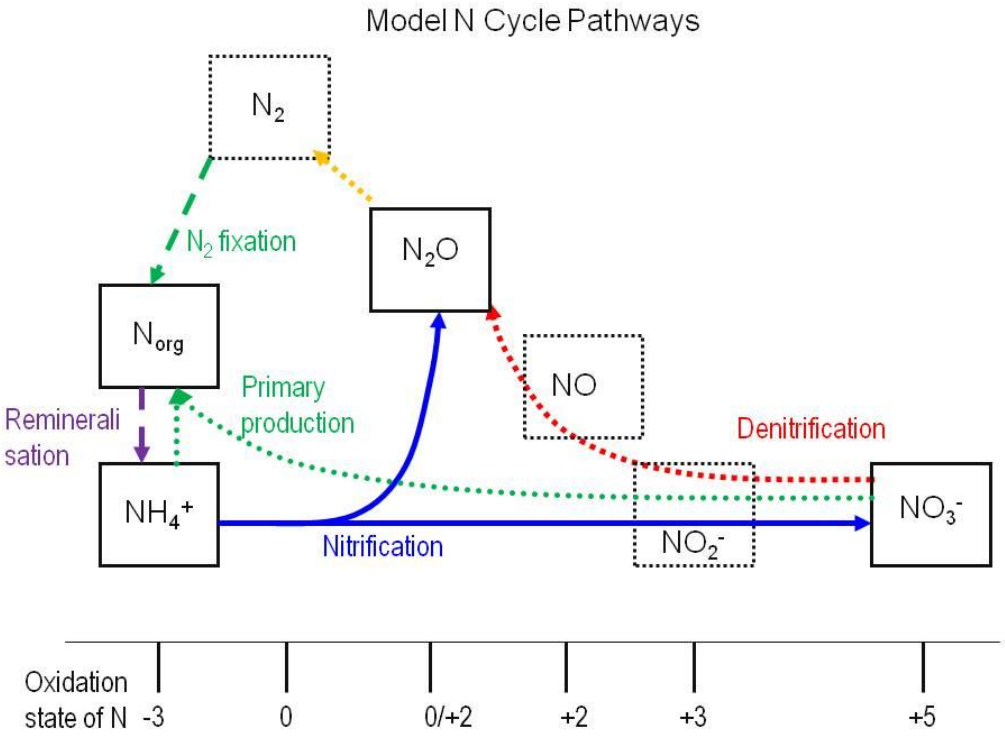

Figure 1: Primary biological pathways of the oceanic nitrogen cycle represented in the model simulations, along with redox states of N. Nitrification occurs in the oxic ocean (blue arrow). Denitrification yields net N_2O production in hypoxic conditions (red arrow) and net N_2O consumption in suboxic conditions (yellow arrow). Only organic nitrogen (N_{org}), NH_4^+, NO_3^- and N_2O are represented as model state variables.

Biogeosciences Discuss., doi:10.5194/bg-2017-193, 2017
Manuscript under review for journal Biogeosciences
Discussion started: 19 May 2017

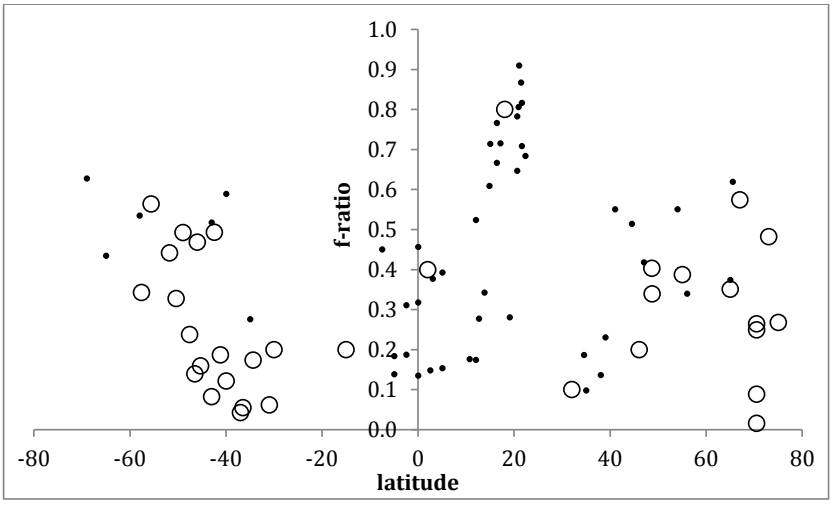

Figure 2: f-ratio ($\rho_{NO_3^-}/(\rho_{NO_3^-}+\rho_{NH_4^+}+\rho_{urea})$) as a function of latitude, from ^{15}N uptake experiments. Small dots were estimated without measuring NH_4^+ or urea concentrations (Prakesh et al. 2008, 2015; Gandhi et al. 2010, 2012). Large dots did not give a significant linear relationship with absolute value of latitude, and were therefore averaged at 0.29 ± 0.18 (Wafar et al. 2004, Varela et al. 2005, 2013 Joubert et al. 2011, Thomalla et al. 2011, Simpson et al. 2013).

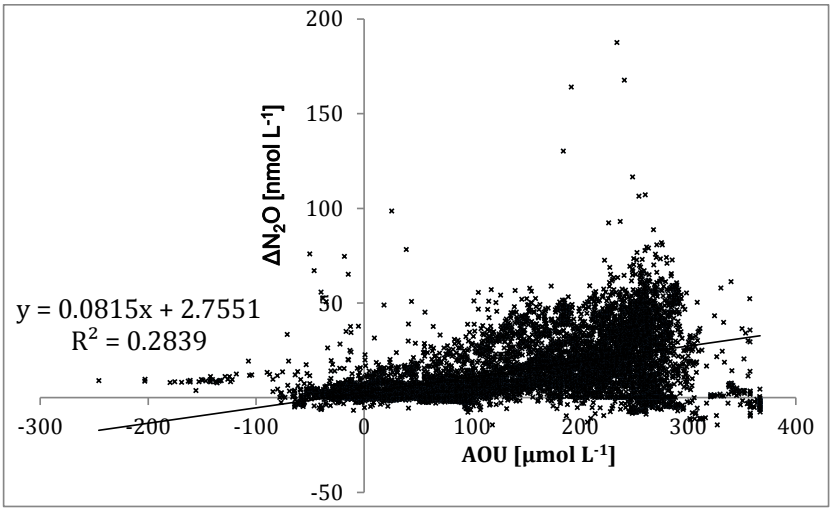

Figure 3: Apparent N_2O production (ΔN_2O nmol L^{-1}) as a function of apparent oxygen utilization (AOU µmol L^{-1}). Calculated from the MEMENTO database (Bange et al. 2009).

Biogeosciences Discuss., doi:10.5194/bg-2017-193, 2017
Manuscript under review for journal Biogeosciences
Discussion started: 19 May 2017

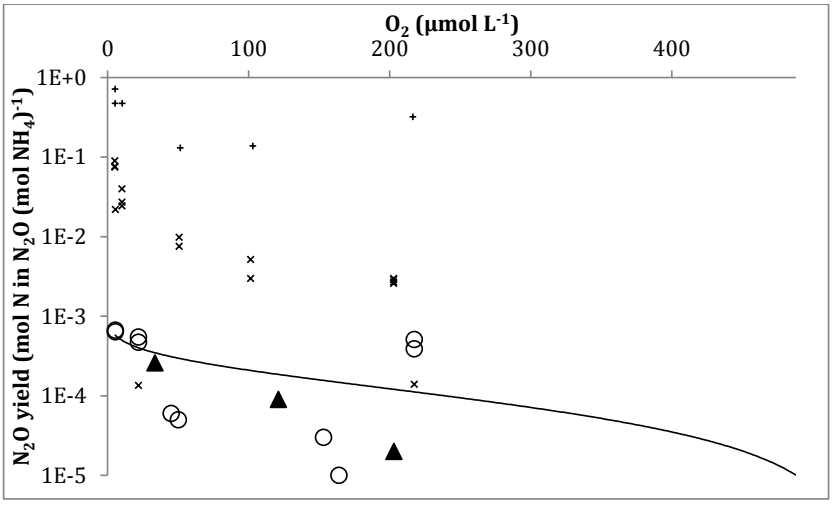

Figure 4: N_2O yield of nitrification (N atom:atom) as a function of O_2 concentration, filled triangles: AOA (Loescher et al. 2012), open circles: AOB at low to medium cell numbers (Frame et al. 2010, Loescher et al. 2012), crosses: marine AOB at high cell numbers (Goreau 1980, Frame et al. 2010), plusses: soil AOB at high cell numbers (Lipschultz 1981). Black line: logarithmic fit to AOA and low to medium cell number AOB (yield = 79.1-12.6·ln(O_2) nmol N in N_2O (µmol NH_4^+)$^{-1}$).

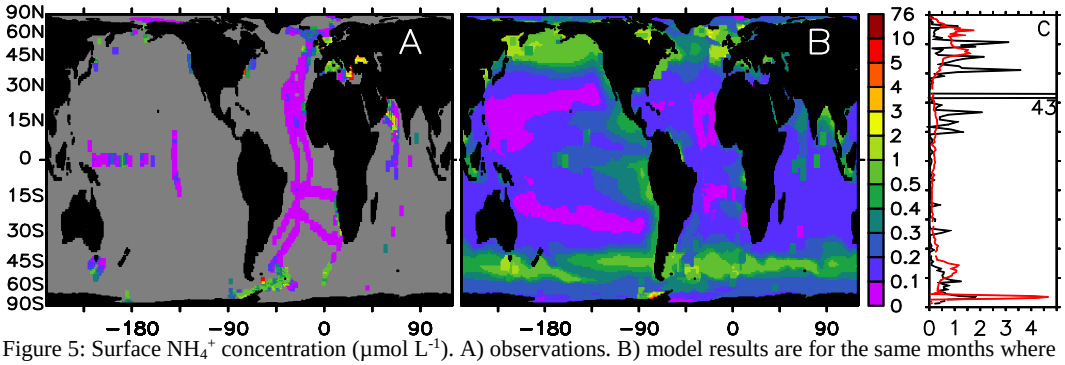

Figure 5: Surface NH_4^+ concentration (µmol L^{-1}). A) observations. B) model results are for the same months where there are observations, and annual averages everywhere else. C) zonal average, black) observations, red) model results. Model results are for the same months and longitudes as the observations.

Biogeosciences Discuss., doi:10.5194/bg-2017-193, 2017
Manuscript under review for journal Biogeosciences
Discussion started: 19 May 2017

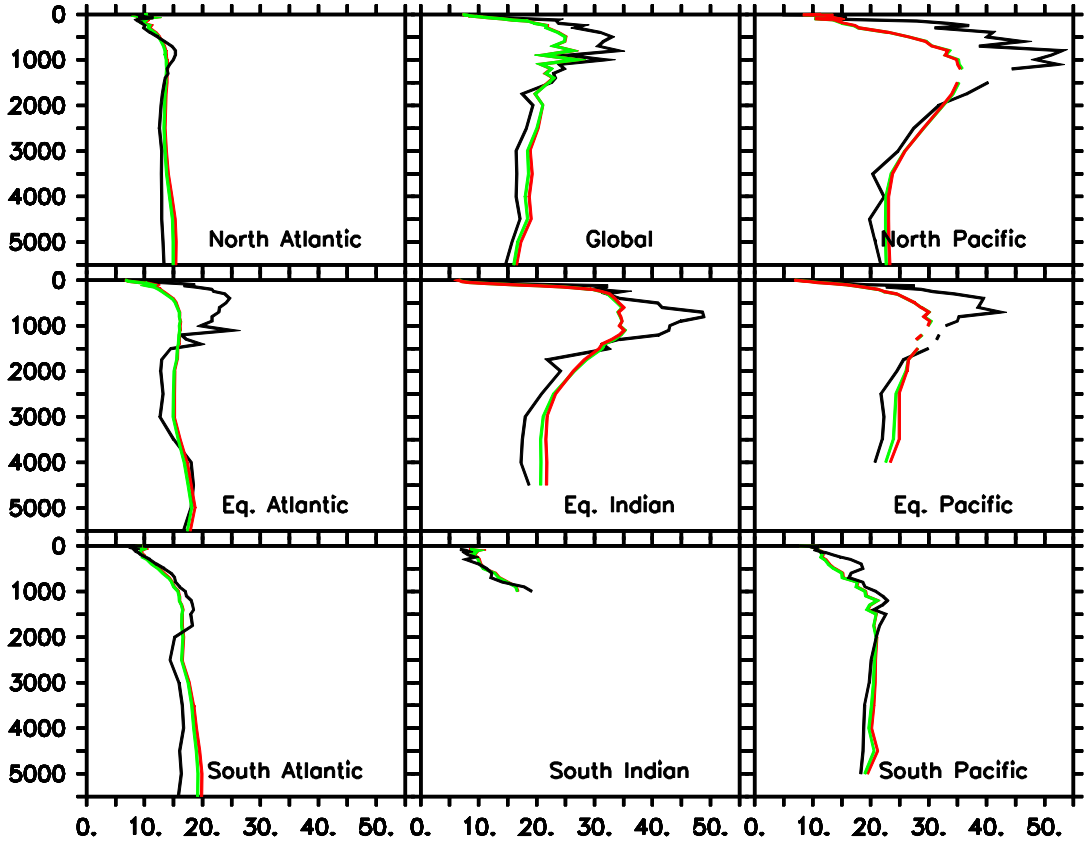

Figure 6: Depth profiles of N_2O concentration (nmol L^{-1}) for different basins. Black lines: observations, Green lines: optimised diagnostic model, Red lines: optimised prognostic model.

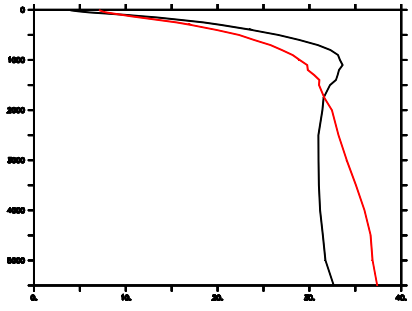

Figure 7: Depth (m.) profile of average NO_3^- concentration (µmol L^{-1}). Black line) WOA2009 synthesis of observations, not interpolated. Red line) Model results sampled at the places where there are observations.

Biogeosciences Discuss., doi:10.5194/bg-2017-193, 2017
Manuscript under review for journal Biogeosciences
Discussion started: 19 May 2017

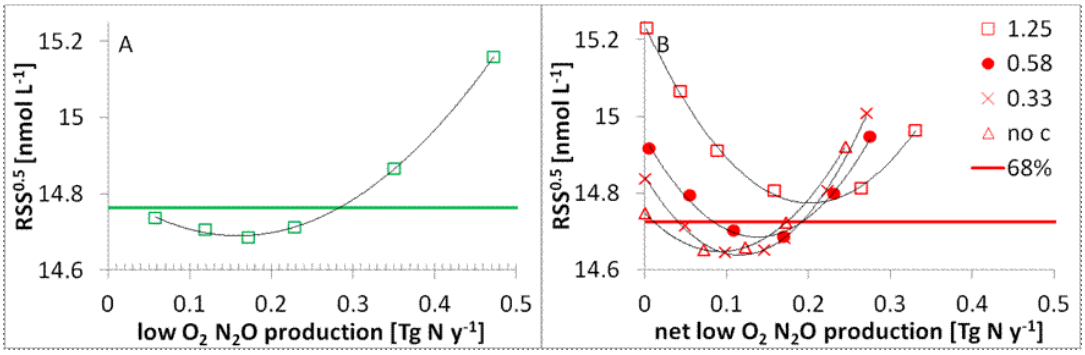

Figure 8: $RSS^{0.5}$ for the two N_2O submodels compared to the N_2O concentration database as a function N_2O production in the low O_2 regions. A) diagnostic submodel, B) net production in the prognostic submodel at different gross production rates, "no c" is with no N_2O consumption i.e. net production = gross production.

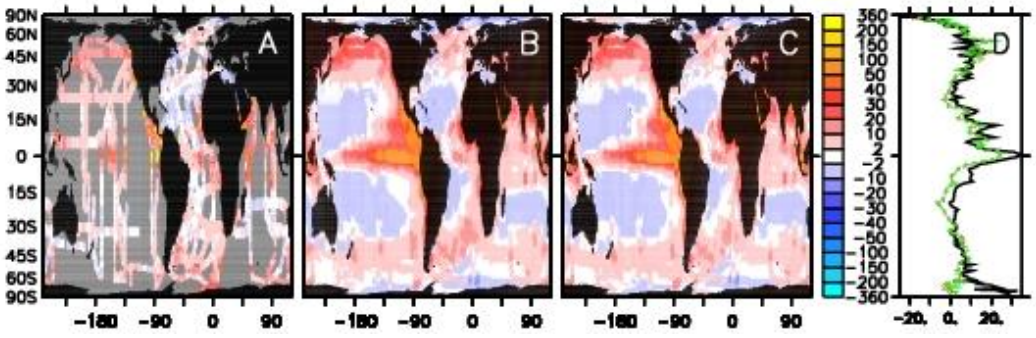

Figure 9: Surface ΔpN_2O [ppb]. A) observations, B) optimised diagnostic model, C) optimised prognostic model. Model results are for the same months where there are observations, and annual averages everywhere else. D) zonal average, Black line: observations, Green dashed: diagnostic model, Red dotted: prognostic model. Model results are for the same months and longitudes as the observations.

Biogeosciences Discuss., doi:10.5194/bg-2017-193, 2017
Manuscript under review for journal Biogeosciences
Discussion started: 19 May 2017

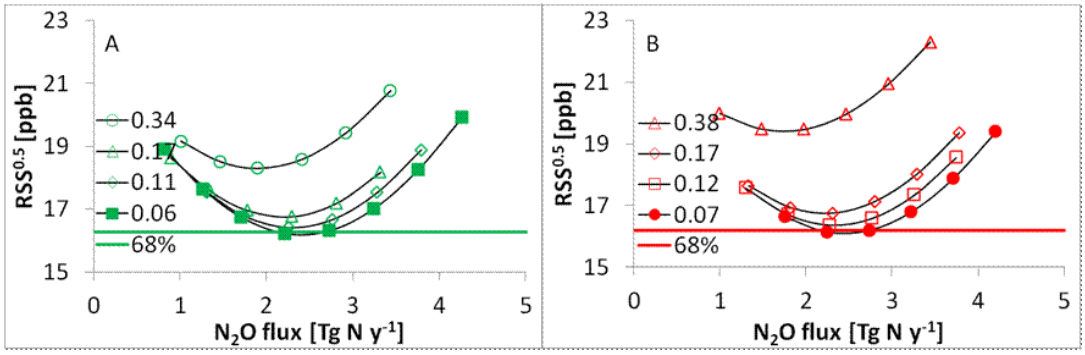

Figure 10: $RSS^{0.5}$ for the two N_2O submodels compared to the ΔpN_2O database as a function of global N_2O flux at different N_2O production rates in the low O_2 regions. A) diagnostic submodel, B) prognostic submodel.

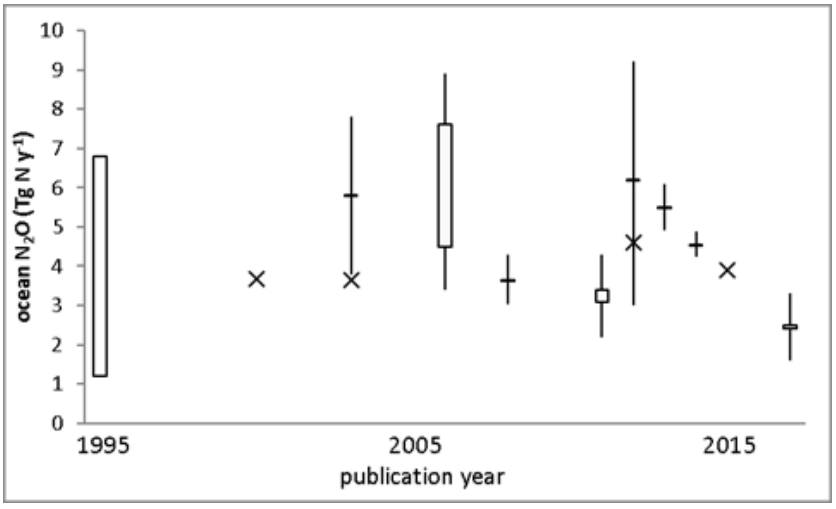

Figure 11: Published estimates of global ocean N_2O production or air-sea exchange. Estimates based on global observational datasets shown as boxes when ranges are given and whiskers if error estimates are given (ocean observations: Nevison et al. 1995, Nevison et al. 2003, Freing et al. 2012 (plotted in 2011), Bianchi et al. 2012, this study; atmospheric inversions: Hirsch et al. 2006, Huang et al. 2008, Thompson et al. 2014 (plotted in 2013), Saikawa et al. 2014), model estimates shown as crosses (Suntharalingam and Sarmiento 2000, Jin and Gruber 2003, Suntharalingam et al. 2012, Martinez-Rey et al. 2015).

Biogeosciences Discuss., doi:10.5194/bg-2017-193, 2017
Manuscript under review for journal Biogeosciences
Discussion started: 19 May 2017

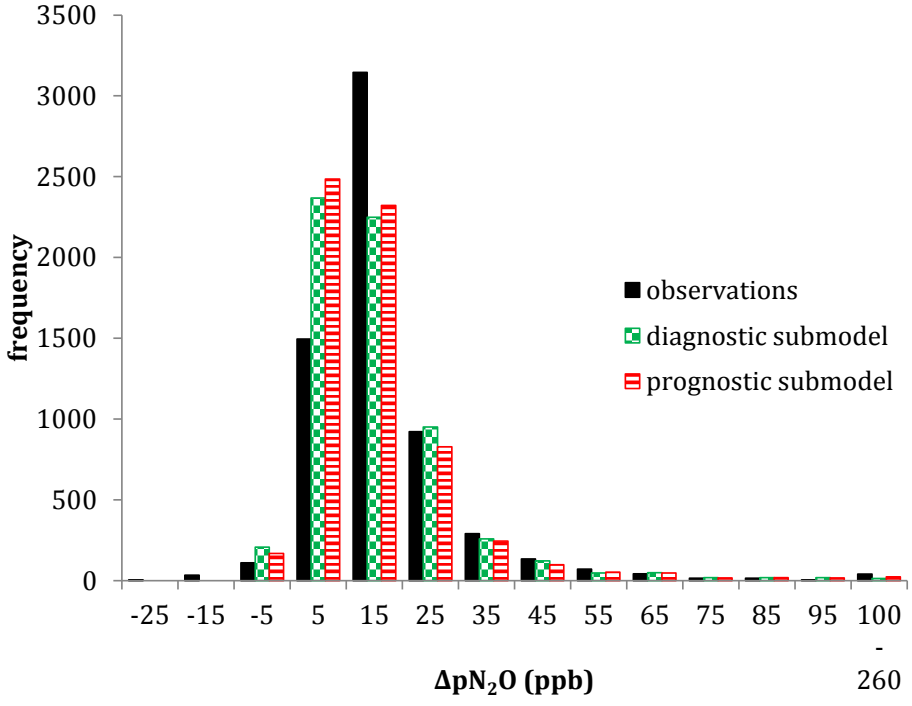

Figure 12: Frequency distribution of ΔpN_2O in the observations (solid black), and the optimised simulations of the diagnostic submodel (green squares) and the prognostic submodel (red lines).